Environmental Science and Pollution Research
https://doi.org/10.1007/s11356-023-29963-y

RESEARCH ARTICLE

Simultaneous removal of four aflatoxins using magnetic nanobentonite as a green and fast sorbent: kinetic, thermodynamic, and isotherm investigation

Marjan Shahinfar[1] · **Naser Hafezi Moghaddas**[1] · **Gholam Reza Lashkaripour**[1] · **Amir Fotovat**[2]

Received: 23 March 2023 / Accepted: 8 September 2023
© The Author(s), under exclusive licence to Springer-Verlag GmbH Germany, part of Springer Nature 2023

Abstract

In the study, an adsorptive removal strategy as a straightforward and fast procedure was developed to remove four aflatoxins, including aflatoxin B1 (AF-B1), aflatoxin B2 (AF-B2), aflatoxin G1 (AF-G1), and aflatoxin G2 (AF-G2). A simple and green sorbent consisting of two components (activated nanobentonite and Fe_3O_4 nanoparticles) was synthesized based on three steps using acidic treatment, ultrasonic procedure, and chemical precipitation method. The sorbent was characterized by several techniques such as FTIR, FESEM, TEM, XRD, and VSM to determine the sorbent structure and morphology. An experimental design based on a central composite design was utilized to optimize factors in the removal of AFs. The optimum values of the factors (pH, sorbent amount, shaking rate) were 6.8, 0.076 g, and 160 rpm, respectively. Three models, including pseudo-first-order, pseudo-second-order, and intra-particle diffusion models, were used to investigate the kinetics of the removal process. The removal of AFs using magnetic nanobentonite was fitted with the pseudo-second-order model better than other models with an equilibrium time lower than 30 min. The thermodynamic data show that the adsorption of AFs on the sorbent is a spontaneous and feasible process due to negative values of the Gibbs-free energy change (ΔG) at different temperatures. Two models (Langmuir and Freundlich models) were chosen to study the isotherm of the removal procedure, indicating that the Freundlich model describes the results better than the Langmuir model. The maximum adsorption capacity of the sorbent for removing AF-B1, AF-B2, AF-G1, and AF-G2 is 357.14, 400.0, 370.37, and 400.0 mg g^{-1}, respectively. The sorbent reusability was also evaluated to study the sorbent's ability for the removal of AFs, indicating that the sorbent was used for 5 cycles without a significant reduction in the ability to remove AFs.

Keywords Magnetic nanobentonite · Adsorptive removal · Aflatoxin · Green sorbent · Kinetic study · Isotherm investigation

Introduction

Aflatoxins (AFs) are a class of organic materials structurally composed of difuranocoumarin and difurocoumarin derivatives, which have a lactone ring and a diene structure with high toxicity which are widely produced by Aspergillus as contaminant in various food samples and can also be found in water sources (Mahato et al. 2019).

Humidity and temperature in a geographical area are two crucial factors in AF production in food samples (Chain et al. 2020). Consumption of AF-contaminated food leads to chronic or acute poisoning in humans. Besides, AFs can be absorbed into humans through inhalation and contact with mucous or skin (Wangia et al. 2019). Adverse effects of exposure to AFs include liver cirrhosis, immune suppression, irritation of mucous membrane, nausea, mutagenesis, carcinogenesis, and growth retardation in children (Aicha et al. 2021; Dai et al. 2017; Negash 2018). In recent years, there has been growing concern over aflatoxin contamination in water environments, particularly in developing countries where inadequate water treatment and sanitation infrastructure can lead to the spread of waterborne diseases.

Responsible Editor: Angeles Blanco

✉ Marjan Shahinfar
Sh.geology7371@gmail.com

[1] Department of Geology, Faculty of Science, Ferdowsi University of Mashhad, Mashhad, Iran

[2] Department of Soil Science, Faculty of Agriculture, Ferdowsi University of Mashhad, Mashhad, Iran

Published online: 04 October 2023

Aflatoxins have been detected in surface water, groundwater, and drinking water sources in many parts of the world, with levels ranging from trace amounts to several hundred micrograms per liter (Picardo et al.2019; Wang et al. 2023).

The safe limit and the maximum acceptable limit of AFs for humans are between 4 and 30 mg kg^{-1} and 20 mg kg^{-1} (U.S. Food and Drug Administration), respectively (Guo et al. 2021; Mahato et al. 2019). Therefore, the removal of AFs in feeds, foods, and water sources is necessary to control their adverse effects on animal and human health (Guo et al. 2021). Various treatment technologies have been introduced and developed, including physical, chemical, and biological methods, as well as a combination of these approaches, to remove contaminants from environmental water sources (de Ilurdoz et al. 2022; Vieira et al. 2020). Some of the main treatment procedures for removing aflatoxin in environmental water sources include adsorption and degradation methods (Wang et al. 2023). Although the degradation of aflatoxins by photocatalysts is an efficient method for this purpose, generally, this method requires UV or gamma rays and oxidizing agents such as ozone or hydrogen peroxide (Wang et al. 2023). Besides, various adsorption methods were presented to remove AFs in water (Samuel et al. 2021), peanut oils (Ji and Xie 2021), vegetable oils (Ma et al. 2021), and rice husk (Li et al. 2022). However, the development of new adsorptive removal procedures with suitable kinetic, absorption capacity, and low price for removing AFs is highly regarded due to their high toxicity and adverse effects of AFs on animal and human health.

The adsorption procedure is an economical, practical, and effective method to remove contaminants in water sources, foods, oils, etc. (Gordi et al. 2020). The advantages of this technique for eliminating pollutants include low cost, simple operation, high efficiency, and availability of many types of sorbents without creating new pollutants (Ghorbani et al. 2021a; Shahmirzadi et al. 2018). The selection, preparation, or synthesis of sorbent in this method is the most critical factor in the success of contaminant removal (Ghorbani et al. 2020). An excellent sorbent has characteristics such as non-toxicity, low cost, high sorption capacity, good reusability, and suitable pollutant sorption at a reasonable time (Farrokhzadeh et al. 2020). Today, green sorbents are highly regarded for removing pollutants because of their agreement with green chemistry (Bulgariu et al. 2019). These sorbents are inexpensive and environmentally friendly and are obtained from natural sources using appropriate processes. Still, the most significant limitation of most of these sorbents is their low sorption capacity, which limits their use (Li et al. 2016). Therefore, modifying the sorbent surface with nanomaterials, changing the sorbent structure with chemical treatment, or functionalizing their surface with proper functional groups enhances the sorption capacity of contaminants by creating appropriate physical and chemical interactions between the modified green sorbent and the pollutants (Ambika et al. 2022; Ibrahim et al. 2019).

Today, the selection and preparation of green sorbents have received much attention to remove pollutants or purify various products due to their cheapness, availability, and compatibility with the environment. Bentonite is a type of clay that is mainly composed of montmorillonite (Atigh et al. 2021). The bentonite is a proper sorbent due to low price, high availability, stability, and adsorption capacity (El-Nagar et al. 2020; Pedram-Rad et al. 2019). The montmorillonite in the bentonite is an aluminum phyllosilicate with microscopic platy grains and high porosity, leading to a high adsorption capacity of bentonite as the sorbent (El-Kheir et al. 2020). Its adsorption capacity is enhanced by the preparation of nanobentonite and increases its surface area. Besides, suitable montmorillonite with three layers, including one layer of alumina in the center covered with two tetrahedral silica layers (Ahmed et al. 2021). The polarity of the Si–O groups on the bentonite surface changes with changing pH that these properties use to selectively adsorb various contaminants through electrostatic attraction.

In this study, a simple and green sorbent (magnetic nanobentonite) was prepared to simultaneously remove four AFs, including aflatoxin B1 (AF-B1), aflatoxin B2 (AF-B2), aflatoxin G1 (AF-G1), and aflatoxin G2 (AF-G2), in water samples. The bentonite was activated by a chemical procedure using an acidic treatment under heating. Sodium bentonite is a type of clay that is widely used for various industrial applications, including as an adsorbent material. One way to activate sodium bentonite is through an acidic treatment, which can modify the structure and properties of the clay to enhance its adsorption capacity. The acidic treatment can target several activation sites in the sodium bentonite, including (i) surface hydroxyl groups: sodium bentonite contains hydroxyl groups (–OH) on its surface that can interact with contaminants through hydrogen bonding. An acidic treatment can increase the number of surface hydroxyl groups, which can enhance the adsorption capacity of the clay; (ii) exchangeable cations: sodium bentonite contains exchangeable cations such as sodium (Na +), calcium (Ca^{2+}), and magnesium (Mg^{2+}) that are loosely bound to the surface of the clay particles. An acidic treatment can remove these exchangeable cations and replace them with hydrogen (H +) ions, which can increase the acidity of the clay and create more adsorption sites. (III) Structural defects: sodium bentonite has a layered structure consisting of montmorillonite sheets that are stacked on top of each other. These sheets can contain structural defects such as broken bonds or missing atoms, which can reduce the adsorption capacity of the clay. An acidic treatment can create new defects or modify existing ones, which can enhance the adsorption capacity of the clay. (IV) Pore size and distribution: sodium bentonite contains pores of various sizes and shapes that

can affect its adsorption capacity. An acidic treatment can modify the size and distribution of these pores, which can increase the surface area available for adsorption (Elgarhy et al 2022; Gandhi et al 2022; Mohajeri et al 2018).

A simple ultrasonic method was used to synthesize nanobentonite from the activated bentonite. Besides, Fe_3O_4 nanoparticles were prepared and penetrated into the nanobentonite pores using an in situ chemical strategy. Using Fe_3O_4 nanoparticles as a sorbent component creates the magnetization property in the sorbent, leading to a fast and simple separation of the sorbent after the absorption procedure (Ghorbani et al. 2021b). The effective factors in the removal of AFs were optimized by central composite design. The kinetics of the removal process was studied according to three models, including pseudo-first-order, pseudo-second-order, and intra-particle diffusion model, under the optimum removal conditions. The isotherm models for removing AFs using magnetic nanobentonite were investigated by Langmuir and Freundlich models. The desorption procedure and the sorbent reusability were also evaluated to study the sorbent's ability for the removal of AFs.

Experimental

Instruments and materials

Aflatoxins were obtained from Farooq Vital Sciences Research Co. Bentonite was purchased from Gohar Khak Khavarmiyaneh Co., Mashhad, Iran, which was obtained from mines in South Khorasan province (Iran). Other materials, including sulfuric acid, nitric acid, iron (II) sulfate heptahydrate, iron (III) nitrate monohydrate, and ammonium hydroxide, were obtained from Merck (Germany).

Aflatoxins were determined using a Knauer HPLC system (Germany) equipped with a prominence fluorescence detector (RF-20A), photoreactor (UVE, LC tech) with a Eurospher 100/5C18 with a diameter of 4.6 mm, length of 250 mm, and ODS of 5 µm. The isocratic mobile phase included two phases: (i) phosphate buffer (0.05 mM, pH 4) and (ii) acetonitrile/methanol with a ratio of 50:50 v/v. The ratio of phase (i) to (ii) was 60:40 v/v. The flow rate was 1.0 mL min^{-1}, and the analysis of AFs was performed at room temperature. The fluorescence detector for the aflatoxins determination was adjusted at excitation and emission wavelengths of 362 and 435 nm, respectively. The morphology and structure of nanobentonite and magnetic nanobentonite were investigated using the FT-IR instrument (Bruker, Germany), transmission electron microscopy (Leo, 912AB, Germany), field emission-scanning electron microscopy (Mira 3 Tescan; Czech Republic), and the X-ray diffraction spectroscopy (EXPLORER XRD, GNR, Italy). The surface area of the samples was determined using Brunauer–Emmett–Teller (BET). The pH of the sample solution was adjusted with a Metrohm 780 pH meter (Herisau, Switzerland).

Synthesis of sorbent

The sorbent was prepared in three steps: (i) activation of sodium bentonite through an acidic treatment, (ii) preparation of activated sodium nanobentonite by sonication wave, and (iii) magnetization of activated nanobentonite using Fe_3O_4 nanoparticles. Briefly, 10.0 g of sodium bentonite was added to an appropriate flask, followed by adding 400.0 mL of a solution containing H_2SO_4 solution (0.1 mol L^{-1}) and HNO_3 solution (0.1 mol L^{-1}) with an equal volume ratio. The mixture was refluxed at 90 ± 5 °C while being stirred at 500 rpm for 3 h. The mixture was cooled, filtered, and finally washed with deionized water three times before drying in a vacuum oven at 80 °C for 24 h.

In the second step, 1.6 g of activated sodium bentonite was added to 100.0 mL of ethanol and sonicated using a sonicate at 50 W for 4 h at room temperature. The ethanol solution was evaporated using an oven at 80 °C for 12 h. Several times, the step was repeated to prepare 20 g of activated sodium nanobentonite. The obtained solid (20 g) was then calcined at 800 °C for 4 h.

In the third step, the activated nanobentonite (15.0 g) was poured into 250.0 mL of an aqueous solution, containing $FeSO_4{\cdot}7H_2O$ (6.25 g) and Fe $(NO_3)_3{\cdot}9H_2O$ (11.80 g), and then sonicated for 20 min at 60 ± 3 °C. The mixture was stirred at 600 rpm for 60 min at 80 °C. The pH of the mixture was raised to 11.0 by adding ammonium hydroxide solution (25%) dropwise while vigorously stirring. The mixture was filtered and washed with deionized water several times, until its pH was approximately neutral. The sorbent was dried in a vacuum oven at 60 °C for 24 h.

Sorbent characterization

FTIR spectra of nanobentonite and magnetic nanobentonite are shown in Fig. 1. A vibration peak at 3433 cm^{-1} is related to kaolinite in nanobentonite, shifted to 3417 cm^{-1} in magnetic nanobentonite. A small vibration peak at 3625 cm^{-1} and 3627 cm^{-1} corresponded to H_2O molecular in nanobentonite and magnetic nanobentonite, respectively. Strong peaks at 1064 cm^{-1} and 547 cm^{-1} are related to montmorillonite in nanobentonite. Another peak at 786 cm^{-1} corresponded to quartz in nanobentonite and magnetic nanobentonite. Finally, a sharp peak at 570 cm^{-1} is related to vibration of Fe–O in magnetic nanobentonite, confirmed to present a magnetic component in the sorbent structure (Ismaeel et al. 2017).

FESEM images of nanobentonite and magnetic nanobentonite are presented in Fig. 2 a and b. The surface

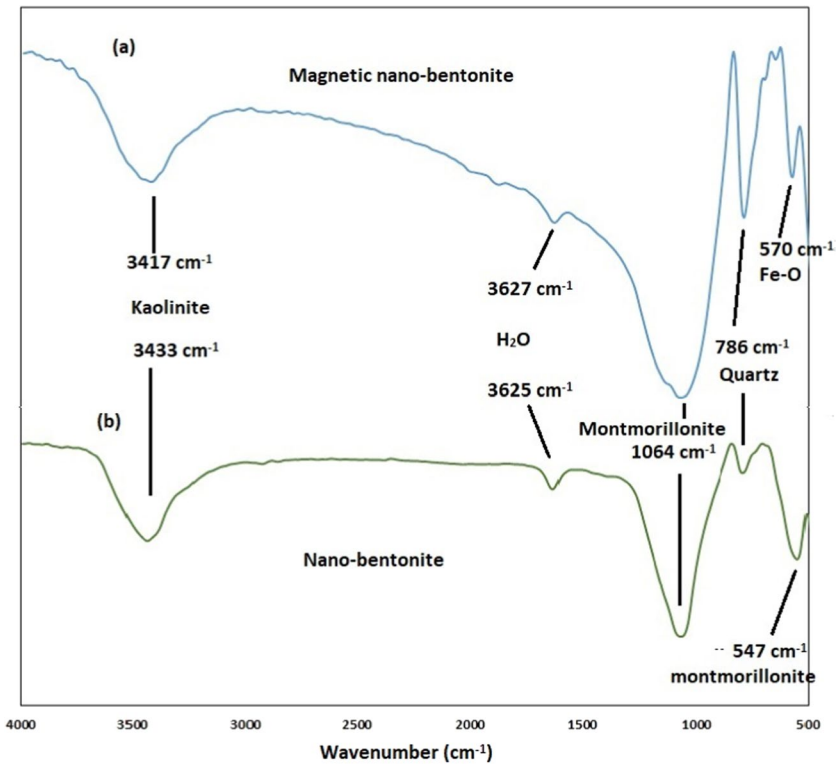

Fig. 1 FTIR spectra of magnetic nano-bentonite (**a**) and nano-bentonite (**b**)

of nanobentonite is almost smooth and flat, covered with spherical nanoparticles of different sizes. The size of these particles is estimated in the range of 20–80 nm. Also, the pores on the nanobentonite surface are very low, which reduces the physical sorption process of AFs (Fig. 2a). In the structure of magnetic nanobentonite, the surface is covered with spherical nanoparticles, which are probably magnetic Fe_3O_4 nanoparticles. The size of these spherical nanoparticles is estimated between 20–40 nm, which due to the magnetic properties of Fe_3O_4 nanoparticles are completely aggregated (Fig. 2b). However, the surface porosity of magnetic nanobentonite is significantly higher than that of nanobentonite, which leads to an increase in the penetration of AFs into the sorbent surface pores for its physical sorption.

EDX patterns of nanobentonite and magnetic nanobentonite are shown in Fig. 2c and d. The nanobentonite is formed from several elements, including calcium, oxygen, gold, silicon, aluminum, and magnesium. The highest weight percentage in the structure of nanobentonite is related to silicon, oxygen, and aluminum, respectively (Fig. 2c; Table S1). In the structure of magnetic nanobentonite, in addition to the mentioned elements, iron with a weight percentage of about 38% is also observed. This high percentage of iron in the structure of magnetic nanobentonite can justify the presence of iron in the sorbent structure and its magnetic properties (Fig. 2d; Table S2).

TEM images of magnetic nanobentonite are shown in Fig. 3(a), indicating that two types of nanoparticles are presented in the magnetic nanobentonite. Large and polygonal particles are less than 90 nm in size, most likely related to nanobentonite, while magnetic Fe_3O_4 nanoparticles are small and spherical particles less than 20 nm in size. Aggregation in the nanoparticles is displayed due to the magnetic properties of Fe_3O_4 nanoparticles.

XRD patterns of nanobentonite and magnetic nanobentonite are presented in Fig. 3(b and c). The XRD pattern of nanobentonite shows that its composite contains quartz, montmorillonite, and muscovite (Fig. 3(b)). Besides, magnetic Fe_3O_4 nanoparticles (JCPDS Card No. 89–0691) in the magnetic nanobentonite with the inverse spinel structure are presented in the sorbent. The diffraction peaks of magnetic Fe_3O_4 nanoparticles are displayed with the planes of (210), (311), (400), (422), (511), and (440) in the sorbent (Fig. 3(c)), indicating the magnetic Fe_3O_4 nanoparticles (JCPDS 79–0418) in the sorbent have a cubic spinel phase.

VSM pattern of magnetic nanobentonite is shown in Fig. 3(d). The results demonstrate that the sorbent has suitable magnetic properties with a saturated magnetization of 8.68 emu g^{-1}, leading to simple separation of sorbent in the presence of a strong magnet.

The BET analysis results for the bentonite and magnetic nanobentonite samples indicate significant differences in their surface area, pore size distribution, and porosity. The

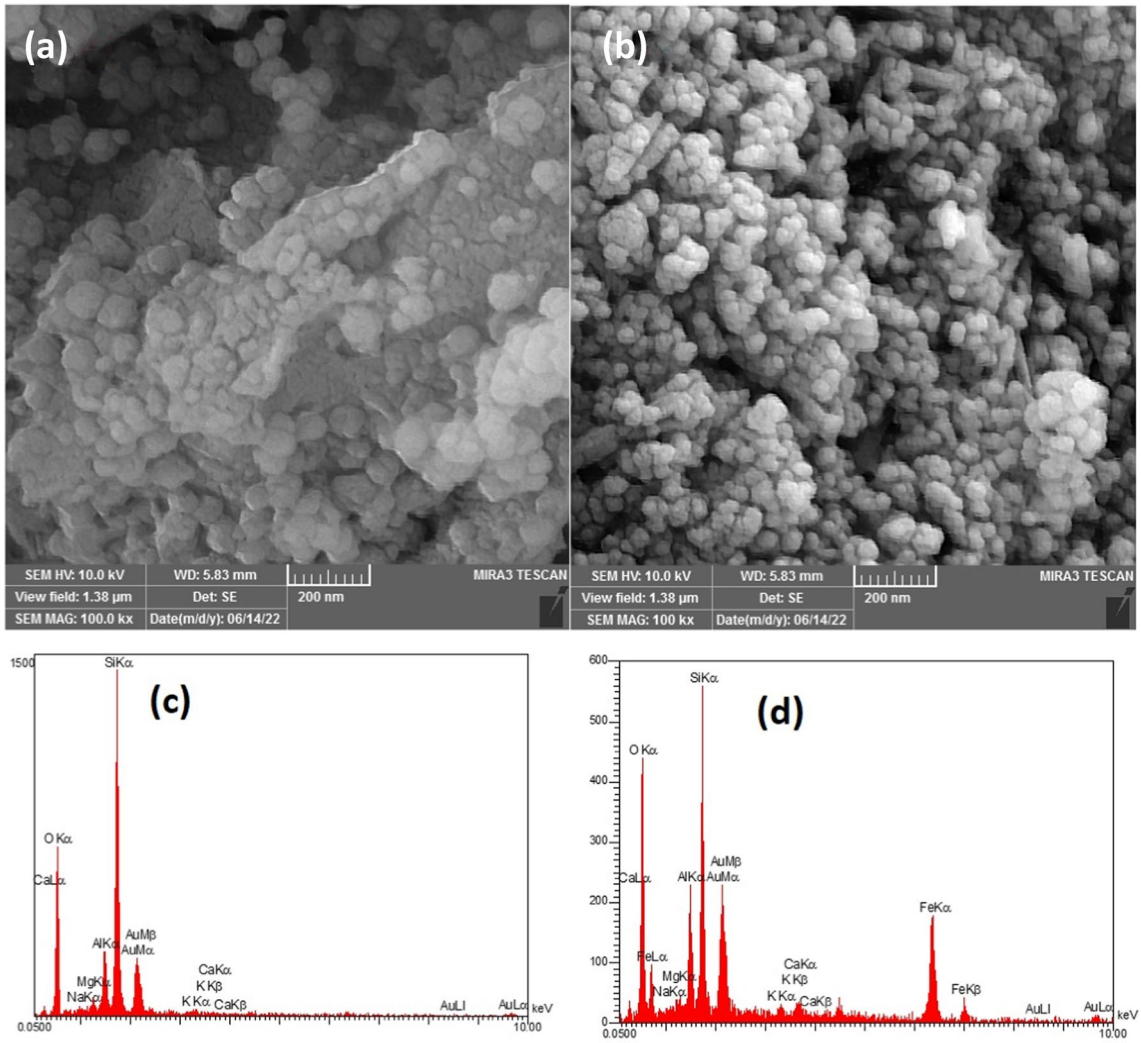

Fig. 2 FESEM images of nanobentonite (**a**) and magnetic nanobentonite (**b**) and EDX patterns of nanobentonite (**c**) and magnetic nanobentonite (**d**)

specific surface area of magnetic nanobentonite (114.84 m^2/g) is significantly higher than that of nanobentonite (76.36 m^2/g). This could be attributed to adding Fe_3O_4 as a sorbent component increases the surface area to interact with AFs. The average pore diameter of magnetic nanobentonite (14.26 nm) is also larger than that of bentonite (9.1 nm) that makes it more suitable to adsorb organic molecules with large size such as AFs. The total pore volume of magnetic nanobentonite (0.409 cc/g) is also higher than that of nanobentonite (0.174 cc/g), indicating that magnetic nanobentonite has a higher porosity compared to nanobentonite to physiosorption of AFs. Overall, the magnetic nanobentonite has a higher specific surface area, larger average pore diameter, and higher porosity than nanobentonite that make it proper to adsorb AFs from the water samples.

Adsorption procedure

The solution of AFs (50.0 mL), including four AFs with a concentration of 20 µg L^{-1}, was poured into an Erlenmeyer. The pH of the solution was adjusted to 6.8 before adding magnetic nanobentonite (0.068 g) as the sorbent. The mixture was shaken at 160 rpm for 30 min. The sorbent was separated using a magnet, and the solution was analyzed by the HPLC method to determine the concentration of each AF. The removal percentage ($R\%$) and the adsorption capacity (q_t) for removing Afs were calculated using the following equations:

$$R(\%) = \left(1 - \frac{C_e}{C_i}\right) * 100 \quad (1)$$

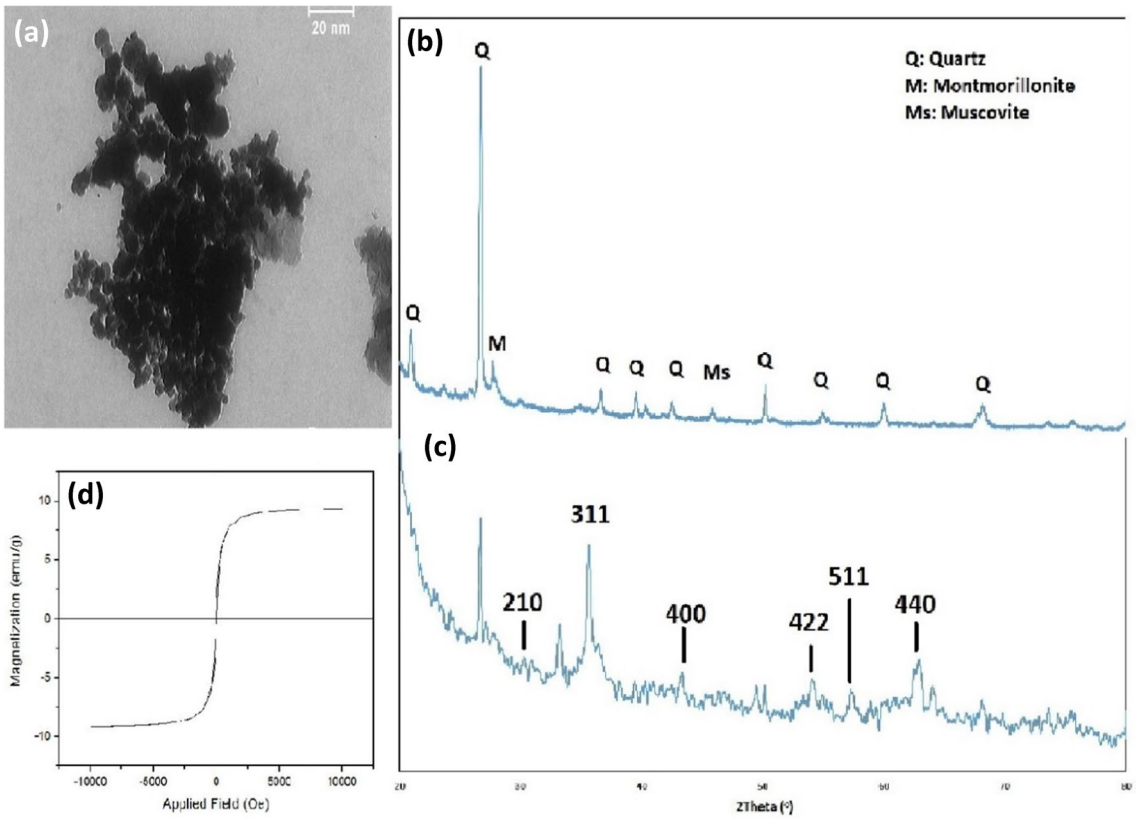

Fig. 3 TEM image of magnetic nanobentonite (**a**), XRD patterns of nano-bentonite (**b**) and magnetic nanobentonite (**c**), VSM pattern magnetic nanobentonite (**d**)

$$q_t = \frac{\left(C_i - C_e\right) * v}{m} \tag{2}$$

where C_e, C_i, V, and m are the equilibrium and initial concentration of AFs, sample volume, and sorbent mass, respectively (Ghorbani et al. 2021a). The adsorption capacity of nanobentonite for AFs compared to nanomagnetic bentonite did not change significantly, while the presence of Fe_3O_4 nanoparticles in magnetic nanobentonite could potentially enhance the reusability and simplicity magnetic separation of the adsorbent material, which could be beneficial for practical applications.

Results and discussion

Adsorption method optimization

The adsorption of AFs using the sorbent is depended on various factors, including pH of the sample, sorbent amount, adsorption time, and shaking rate. Adsorption time and temperature were individually investigated in kinetic and thermodynamic studies of the adsorption process. Three factors of pH, sorbent amount, and shaking rate were optimized using an experimental design. For this purpose, a central composite design, including twenty experimental runs, was utilized to optimize these factors. The runs were performed in random order with three times replication of each run under the same conditions to calculate the mean of R% for each run. The temperature and time were constant at 23 ± 2 and 60 min, respectively. The factors, design, and removal percentages are presented in Table 1. The obtained *R%* was analyzed using one-way ANOVA at a 95% confidence interval (Table 2). The *p*-values of the model and lack of fit are lower and higher than 0.05, respectively, showing that the provided model in the design is meaningful in describing the results. All factors have significant effects on the removal of AFs because the obtained *p*-value of each factor is lower than 0.05 (α-level at a 95% confidence interval). Besides, all interactions between factors are meaningful in the removal procedure, except the interaction between pH and shaking rate is not significant due to the *p*-value greater than 0.05. Three-dimensional surface plots of the significant interactions are presented in Fig. 4, in which two factors were simultaneously changed to determine *R%* while the third factor is fixed in its mean value. The *R%* of AFs using the sorbent increases sharply with the simultaneous increase of pH and sorbent amount and then is almost constant (Fig. 4a).

Table 1 Factors and central composite design for optimizing the factors

Factor	Name	Units	Type	Minimum	Maximum	Mean	Standard deviation
A	Sorbent amount	mg	Numeric	0.0200	0.1000	0.0600	0.0290
B	pH	–-	Numeric	4.00	8.00	6.00	1.45
C	Shaking rate	rpm	Numeric	100.00	200.00	150.00	36.27
Standard run			Run	*A*	*B*	*C*	*R*%
3			1	0.02	8	100	52.05
5			2	0.02	4	200	69.52
7			3	0.02	8	200	63.38
9			4	0.02	6	150	71.92
1			5	0.02	4	100	47.81
17			6	0.06	6	150	98.46
11			7	0.06	4	150	68.45
13			8	0.06	6	100	90.13
18			9	0.06	6	150	91.76
19			10	0.06	6	150	94.79
16			11	0.06	6	150	95.23
15			12	0.06	6	150	98.16
12			13	0.06	8	150	90.47
20			14	0.06	6	150	97.23
14			15	0.06	6	200	93.41
8			16	0.1	8	200	85.85
4			17	0.1	8	100	87.73
10			18	0.1	6	150	92.53
2			19	0.1	4	100	59.16
6			20	0.1	4	200	62.05

Table 2 Analysis of variance for evaluating the obtained *R*%

Source	Sum of squares	*df*	Mean square	*F*-value	*p*-value	Significant
Model	5252.15	9	583.57	57.63	< 0.0001	+
A-Sorbent amount	682.94	1	682.94	67.44	< 0.0001	+
B-pH	525.48	1	525.48	51.89	< 0.0001	+
C-Shaking rate	139.20	1	139.20	13.75	0.0041	+
AB	368.15	1	368.15	36.36	0.0001	+
AC	128.24	1	128.24	12.66	0.0052	+
BC	28.69	1	28.69	2.83	0.1232	–
A^2	404.60	1	404.60	39.95	< 0.0001	+
B^2	610.08	1	610.08	60.25	< 0.0001	+
C^2	18.23	1	18.23	1.80	0.2094	–
Residual	101.27	10	10.13			
Lack of fit	69.02	5	13.80	2.14	0.2116	–
Pure error	32.24	5	6.45			
Cor Total	5353.41	19				

Increasing the sorbent amount leads to a rise in the number of active sites at the sorbent surface for interaction with AFs. Also, the change in pH strongly affects the *R*% of AFs by changing the polarity of the functional groups at the sorbent surface and AFs. In Fig. 4b, the *R*% of AFs increases gradually with the simultaneous increase of sorbent amount and shaking rate and reduces afterward. An increase in shaking rate increases the mass transfer of the sorbent and AFs in solution; as a result, the interaction between the sorbent and AFs and the *R*% of AFs increases.

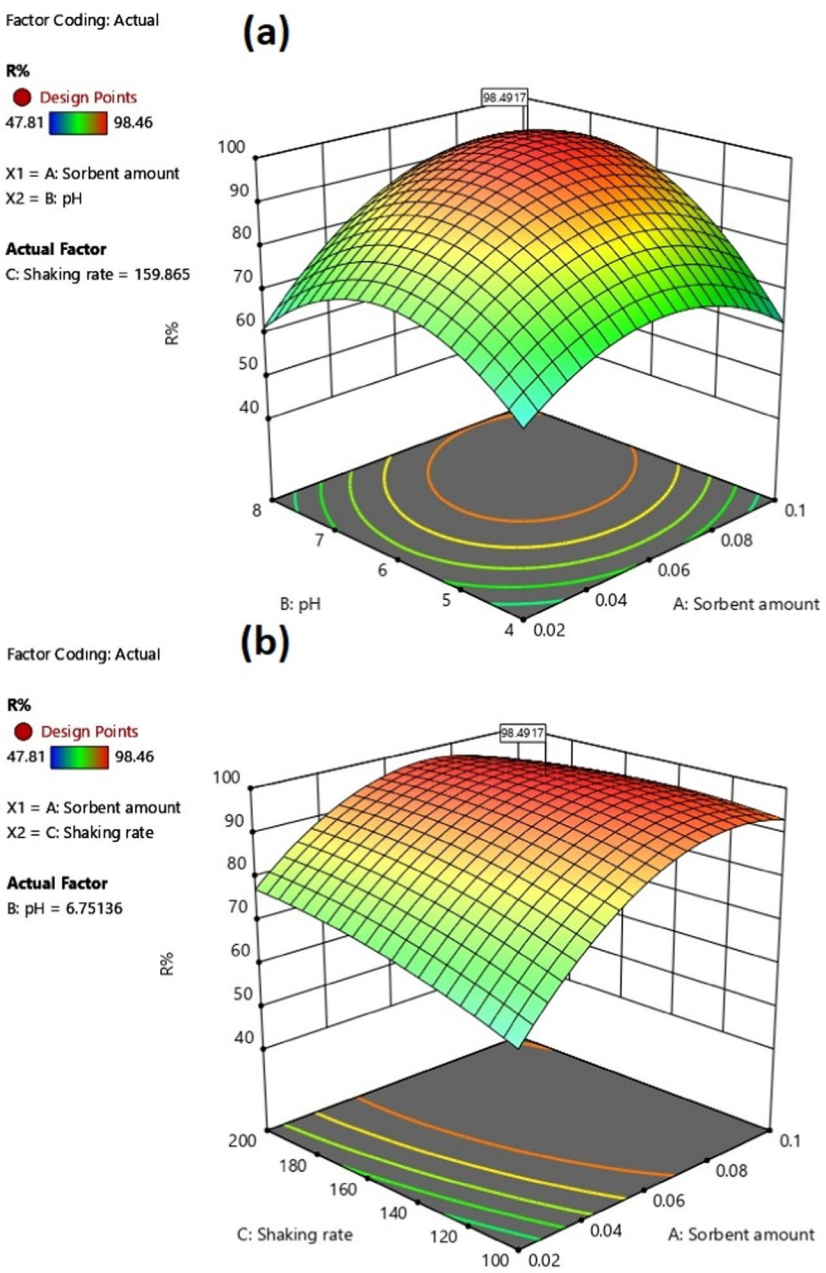

Fig. 4 Surface plots of the significant interactions of factors in the removal of AFs, pH and sorbent amount (**a**), shaking rate and sorbent amount (**b**)

The relationship between the *R*% of AFs as a dependent factor and the change in factors as independent factors with a quadratic equation can be described as follows:

$$R\% = 95.3048 + 8.264 * A + 7.249 * B + 3.731 * C + 6.78375 * AB - 4.00375 * AC - 1.89375 * BC - 12.1295 * A^2 - 14.8945 * B^2 - 2.57455 * C^2 \quad (3)$$

R-squared and adjusted *R*-squared of the equation were 0.9811 and 0.9641, indicating that the equation fitted well with the responses. In addition, a high predicted *R*-squared (0.8862) shows that the equation is able to predict the *R*% of AFs by changing the values of the factors significantly. The linear coefficient of *A* (sorbent amount) is the highest in the equation, indicating that sorbent amount has the most positive effect on the *R*% of AFs. The results reveal that although all three factors have a significant impact on the *R*% of AFs, the effect of the sorbent amount is the greatest. The optimum value of each factor was determined using the equation and design, in which the maximum of *R*% of AFs was selected as a goal. The optimum value of the sorbent amount, pH, and shaking rate was 0.076 g, 6.8, and 160 rpm, respectively (Fig. S3).

Table 3 Kinetic models for the adsorption of AFs

Model		AF-B1	AF-B2	AF-G1	AF-G2
Pseudo-first-order	Equation	$Y=-0.0033x+2.5986$	$Y=-0.0051x+2.5281$	$Y=-0.0047x+2.5593$	$Y=-0.0045x+2.5834$
	R^2	0.9248	0.946	0.9273	0.9652
	q_e (mg g^{-1})	396.82	337.36	362.49	383.18
	$K_1 * 10^{-3}$ (min^{-1})	7.6	11.7	10.8	10.4
Pseudo-second-order	Equation	$Y=0.0064x+0.0251$	$Y=0.006x+0.0368$	$Y=0.0059x+0.0349$	$Y=0.006x+0.0412$
	R^2	0.99	0.9902	0.9869	0.9905
	q_e (mg g^{-1})	156.25	166.67	169.49	166.67
	$K * 10^{-3}$ (g mg^{-1} min^{-1})	1.63	0.978	0.997	0.874
Intra-particle diffusion	Equation	$Y=18.842x+49.24$	$Y=23.361x+25.491$	$Y=23.671x+27.549$	$Y=23.993t+19.7$
	R^2	0.9464	0.9689	0.9547	0.9819
	k_{dif} (mg g^{-1} $min^{-1/2}$)	18.842	23.361	23.671	23.993
	C	49.24	25.49	27.549	19.7

Kinetic study

The adsorption of AFs on the sorbent was investigated at room temperature for 5–20 min to evaluate the kinetic model. The concentration of AFs, pH, temperature, and shaking rate were 20 µg L^{-1}, 6.8, 23 ± 1 °C, and 160 rpm, respectively. For this purpose, three kinetic models were chosen to study the obtained results. The linear form of the kinetic equations, including pseudo-first-order (q5), pseudo-second-order (q6), and intra-particle diffusion (q7) model, for this investigation are as follows (Ghorbani et al. 2021a):

$$log\left(q_e - q_t\right) = logq_e - \frac{k_1 t}{2.303} \tag{4}$$

$$\frac{t}{q_t} = \frac{1}{k_2 q_e^2} + \frac{1}{q_e} t \tag{5}$$

$$q_t = k_i * t^{\frac{1}{2}} + C \tag{6}$$

where k is the rate constant for each model in the equations. The results are summarized in Table 3, indicating the best model to fit the results for describing the absorption process of AFs is the pseudo-second-order model because the obtained R-squared is the highest for the model compared to other models. The results showed that the removal of AFs was increased with increasing time up to 25 min and then remained almost constant afterward. Therefore, the removal process reaches equilibrium for a time lower than 30 min, indicating that the removal of AFs using the sorbent is a fast process. Besides, a better fit of the results with the pseudo-second-order model than other models shows that the process of removal of AFs on the sorbent occurs mainly through strong physical or chemical interactions and the penetration of AFs into the sorbent pores has little effect on their removal. These results are confirmed by the low R^2 obtained in the intra-particle diffusion model except for the AF-G2. A high R^2 value (0.9819 and 0.9905) for the intra-particle diffusion and pseudo-second-order model to remove AF-G2 indicates that the removal of AF-G2 is affected by its physical and chemical interactions with magnetic nanobentonite as sorbent and also its penetration into the sorbent pores. Also, the penetration of AFs into the magnetic nanobentonite pores is not the rate-controlling step for removing AFs using the sorbent because the Weber–Morris plots (intra-particle diffusion model) do not pass through the origin and the C-values in the equations are greater than zero (Ghorbani et al. 2017).

Thermodynamic study

Enthalpy and entropy are critical thermodynamic parameters whose changes are considered for evaluating the nature and feasibility of chemical reaction and sorption procedures by determining the Gibbs-free energy (ΔG). For this purpose, the enthalpy change (ΔH) and entropy change (ΔS) were calculated by investigating changes in pollutant absorption using sorbent versus temperature to determine ΔG in various temperatures according to the following equations:

$$K_d = \frac{q_t}{C_e} \tag{7}$$

$$lnK_d = \frac{\Delta S}{R} - \frac{\Delta H}{RT} \tag{8}$$

$$\Delta G = \Delta H - T\Delta S \tag{9}$$

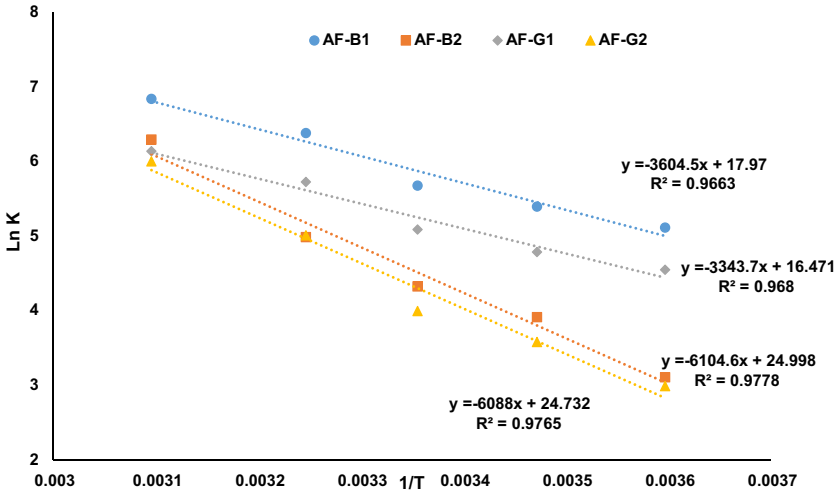

Fig. 5 Effect of temperature on the adsorption of AFs on the magnetic nanobentonite

where K_d, R, and T are the equilibrium constant (L g^{-1}) for the adsorption process, the universal gas constant (8.314 J mol^{-1} K^{-1}), and the absolute temperature (K). The standard enthalpy changes ($\Delta H°$) and entropy changes ($\Delta S°$) were calculated by drawing ln K_d versus T^{-1} using slope and intercept in Eq. 9, respectively (Fig. 5). The thermodynamic data are presented in Table 4. $\Delta H°$s were positive for the removal of AFs with a higher value than 20 kJ mol^{-1}, indicating that the adsorption of AFs on the sorbent is an endothermic process with a chemical in nature. $\Delta H°$s for adsorption of AF-G1 and AF-G2 are higher than AF-B1 and AF-B2, showing that interactions between AF-G1 and AF-G2 with sorbent are stronger than AF-B1 and AF-B2. However, an increase in the adsorption of AFs showed by increasing the temperature of the solution. $\Delta S°$s for adsorbing AFs on the sorbent are positive leading to an increase in the randomness at the sample solution and the sorbent surface interface due to the adsorption of AFs on the sorbent. Besides, negative values of the Gibbs-free energy change (ΔG) at different temperatures in the range of 278–323 K indicated that the adsorption of AFs on the sorbent is a spontaneous and feasible process.

Table 4 Thermodynamic parameters for the adsorption of AFs

Thermodynamic parameters		AF-B1	AF-B2	AF-G1	AF-G2
ΔH (Kjmol^{-1})		29.968	27.800	50.754	50.616
ΔS (Jmol^{-1} k^{-1})		149.403	136.940	207.833	205.6218
ΔG (Kj mol^{-1})	T (K)				
	278	− 11.443	− 10.286	− 7.07	− 6.652
	288	− 12.933	− 11.656	− 9.15	− 8.712
	298	− 14.423	− 13.026	− 11.23	− 10.772
	308	− 15.913	− 14.396	− 13.31	− 12.832
	323	− 18.148	− 16.451	− 16.43	− 15.922

Isotherm study

Two models, including Langmuir and Freundlich adsorption isotherm models, were selected to investigate the isotherm of AF removal. The concentration of AFs was changed in the range of 20–50 µg L^{-1}, in which the pH of the solution was adjusted to 6.8. The sorbent amount, shaking rate, and adsorption time were 0.076 g, 160 rpm, and 30 min, respectively. The Langmuir (Eq. 11) and Freundlich (Eq. 12) isotherm models were evaluated with linear equations for removing AFs as follows:

$$\frac{C_e}{q_e} = \frac{C_e}{q_{max}} + \frac{1}{bq_{max}} \tag{10}$$

$$lnq_e = lnk_f + \frac{1}{n} lnC_e \tag{11}$$

where b and q_{max} in the Langmuir model are Langmuir constant (L mg^{-1}) and maximum monolayer sorption capacity (mg g^{-1}). Besides, two parameters (n and k_f) in the Freundlich model are adsorption intensity and Freundlich constants (mg g^{-1}). The results are presented in Table 4, and the best model to describe the removal of AFs was selected using the obtained R^2 for two models. Therefore, the Freundlich model describes the results better than the Langmuir model because the obtained R^2 for the Freundlich model is higher than the Langmuir model for removing all AFs using the sorbent. These results indicated the magnetic nanobentonite as sorbent has a heterogeneous surface leading to multilayer adsorption of AFs on the sorbent surface. The heterogeneous surface of the magnetic nanobentonite may be due to the preparation of sorbent composite from two nanomaterials with different sizes and structures. These differences are also shown in the SEM and TEM images of the sorbent (Figs. 2 and 3). The favorability of the adsorption

Table 5 Isotherm model for the adsorption of AFs

Model		AF-B1	AF-B2	AF-G1	AF-G2
Langmuir	Equation	$Y=0.0028x+0.00661$	$Y=0.0025x+0.1771$	$Y=0.0027x+0.0862$	$Y=0.0025x+0.2313$
	R^2	0.9501	0.9538	0.9575	0.9348
	q_e (mg g^{-1})	357.14	400.0	370.37	400.0
	b	0.424	0.014	0.031	0.011
	R_l	0.9218–0.028	0.989–0.459	0.988–0.278	0.988–0.510
Freundlich	Equation	$Y=0.482x+1.9378$	$Y=0.486x+1.9215$	$Y=0.4837x+1.9336$	$Y=0.487x+1.9118$
	R^2	0.9909	0.9906	0.9909	0.9906
	K_f	5.04	4.97	5.02	4.93
	n	2.07	2.06	2.07	2.05

procedure evaluates using the adsorption intensity (n) in the Freundlich model. The n-value of 1–10 indicates the favorable absorption of AFs on the magnetic nanobentonite. The n-values for the adsorption of AF-B1, AF-B2, AF-G1, and AF-G2 are 2.07, 2.06, 2.07, and 2.05, indicating the adsorption process for all AFs on the sorbent are favorable. The Freundlich constants for the AFs adsorption are in the range of 4.93–5.04. The high values of K_f show the adsorptions of AFs occur with high affinity on the sorbent. The Langmuir model was used to calculate the maximum adsorption capacity of the sorbent. The q_{max} values for removing AF-B1, AF-B2, AF-G1, and AF-G2 are 357.14, 400.0, 370.37, and 400.0 mg g^{-1}, respectively. Also, the favorability of the adsorption procedure can be investigated based on the Langmuir model using the dimensionless constant separation factor (R_L) that was calculated according to the following equation:

$$R_l = \frac{1}{1 + bC_e} \tag{12}$$

The favorable adsorption occurs for a R_L-value between 0 and 1. Besides, the adsorption is linear for the R_L-value of 1 and irreversible for the R_L-value of 0. The R_L-values of AFs adsorption are between 0 and 1, indicating that the adsorption is favorable (Table 5).

Reusability of sorbent

The desorption of AFs from the magnetic nanobentonite as sorbent was carried out to study the sorbent reusability. After adsorbing AFs on the sorbent, the desorption procedure was performed using 10.0 mL of sodium hydroxide solution (0.1 M) under sonicating for 5 min. The sorbent was then separated using a magnet and washed three times using distilled water before reusing it to adsorb AFs. Comparison of VSM, XRD after 5 reuses of nanocomposite showed deviations of less than 5% in its structure. Thus, sorbent was used for 5 cycles without significant reduction in the ability to remove AFs (Table 6), indicating that the sorbent has high stability in the sample solution for AF removal with a high removal efficiency under a low adsorption time.

Table 6 Reusability of the sorbent for the adsorption of AFs ($n=3$)

Cycle	Removal percentage ± S			
	AF-B1	AF-B2	AF-G1	AF-G2
1	95.49 ± 2.36	95.83 ± 2.19	94.32 ± 2.54	96.11 ± 2.22
2	94.74 ± 2.45	94.02 ± 2.28	93.94 ± 2.63	94.26 ± 2.27
3	92.16 ± 2.71	92.73 ± 2.56	91.97 ± 2.65	92.77 ± 2.55
4	89.45 ± 2.93	90.11 ± 2.84	88.53 ± 2.88	90.31 ± 2.72
5	86.09 ± 3.02	85.47 ± 3.15	84.38 ± 2.96	84.95 ± 2.86
6	76.94 ± 4.21	77.31 ± 3.87	75.02 ± 3.75	78.53 ± 3.64

Conclusion

In the study, the removal of four AFs was investigated using an adsorptive removal strategy to a straightforward and fast procedure. Magnetic nanobentonite was prepared as a simple and green sorbent under three steps, including activation of bentonite using acidic treatment, preparation of nanobentonite based on an ultrasonic procedure, and magnetization of nanobentonite with Fe_3O_4 nanoparticle according to a chemical precipitation method. The sorbent was characterized by FTIR, FESEM, TEM, XRD, and VSM methods to determine the sorbent structure and morphology. Influential factors in the removal of AFs were investigated by central composite design to reduce the experimental runs and reagent consumption and study the interaction between factors. The kinetics of the removal process was studied according to three models, including pseudo-first-order, pseudo-second-order, and intra-particle diffusion model, under the optimum removal conditions. The removal of AFs using magnetic nanobentonite was fitted with the pseudo-second-order model better than other models, showing that the process

occurs mainly through strong physical or chemical interactions between AFs with the sorbent. The thermodynamic studies indicated that the adsorption of AFs on the sorbent is a spontaneous and feasible process due to negative values of the Gibbs-free energy change (ΔG) at different temperatures in the range of 278–323 K. Also, the investigation of isotherm models for removing AFs demonstrates that the Freundlich model describes the results better than the Langmuir model, and so, the sorbent has a heterogeneous surface, leading to multilayer adsorption of AFs on the sorbent surface. The sorbent reusability was also evaluated to study the sorbent's ability for the removal of AFs, indicating that the sorbent was used for 5 cycles without a significant reduction in the ability to remove AFs.

Supplementary Information The online version contains supplementary material available at https://doi.org/10.1007/s11356-023-29963-y.

Author contribution All authors contributed to the study conception and design. Material preparation, data collection, and analysis were performed by Marjan Shahinfar, Naser Hafezi Moghaddas, Gholam Reza Lashkaripour, and Amir Fotovat. The first draft of the manuscript was written by Marjan Shahinfar, and all authors commented on previous versions of the manuscript. All authors read and approved the final manuscript and that there are no other persons who satisfied the criteria for authorship but are not listed. The authors further confirm that the order of authors listed in the manuscript has been approved by all of us.

Funding This research was funded by Department of Geology, Faculty of Science, Ferdowsi University of Mashhad under the grant number of 56299.

Data availability The data that supports the findings of this study are available in the manuscript and supplementary material of this article.

Declarations

Ethical approval This article does not contain any studies with human participants or animals performed by any of the authors.

Consent to participate Not applicable.

Consent for publication The consent of all the authors of this article has been obtained for submitting the article to the journal.

Conflict of interest The authors declare no competing interests.

References

Ahmed A, Ayad MI, Eledkawy MA, Darweesh M, Elmelegy EM (2021) Removal of iron, zinc, and nickel-ions using nano bentonite and its applications on power station wastewater. Heliyon 7:e06315

Aicha Y, Cisse H, Oumarou Z, Nikiema F, Traore Y, Savadogo A (2021) Reduction of aflatoxins and microorganisms in the koura-koura produced in Burkina Faso with spices and aromatic leaves. J Food Technol 8:9–17

Ambika S, Kumar M, Pisharody L, Malhotra M, Kumar G, Sreedharan V, Singh L, Nidheesh P, Bhatnagar A (2022) Modified biochar as a green adsorbent for removal of hexavalent chromium from various environmental matrices: mechanisms, methods, and prospects. Chem Eng J 439:135716

Atigh ZBQ, Sardari P, Moghiseh E, Lajayer BA, Hursthouse AS (2021) Purified montmorillonite as a nano-adsorbent of potentially toxic elements from environment: an overview. Nanotechnol Environ Eng 6:12

Bulgariu L, Escudero LB, Bello OS, Iqbal M, Nisar J, Adegoke KA, Alakhras F, Kornaros M, Anastopoulos I (2019) The utilization of leaf-based adsorbents for dyes removal: a review. J Mol Liq 276:728–747

Chain EPOCITF, Schrenk D, Bignami M, Bodin L, Chipman JK, del Mazo J, Grasl-Kraupp B, Hogstrand C, Hoogenboom L, Leblanc JC (2020) Risk assessment of aflatoxins in food. EFSA Journal 18:e06040

Dai Y, Huang K, Zhang B, Zhu L, Xu W (2017) Aflatoxin B1-induced epigenetic alterations: an overview. Food Chem Toxicol 109:683–689

de Ilurdoz MS, Sadhwani JJ, Reboso JV (2022) Antibiotic removal processes from water & wastewater for the protection of the aquatic environment-a review. J Water Process Eng 45:102474

Elgarhy AH, Mahran BN, Liu G, Salem TA, ElSayed EE, Ibrahim LA (2022) Comparative study for removal of phosphorus from aqueous solution by natural and activated bentonite. Sci Rep 12(1):19433

El-Kheir A, El-Ghany A, Fahmy MM, Aboras S, El-Gabry L (2020) Functional finishing of polyester fabric using bentonite nanoparticles. Egypt J Chem 63:85–99

El-Nagar DA, Massoud SA, Ismail SH (2020) Removal of some heavy metals and fungicides from aqueous solutions using nano-hydroxyapatite, nano-bentonite and nanocomposite. Arab J Chem 13:7695–7706

Farrokhzadeh S, Razmi H, Jannat B (2020) Application of marble powder as a potential green adsorbent for miniaturized solid phase extraction of polycyclic aromatic hydrocarbons from water samples. Sep Sci Technol 55:2737–2745

Gandhi D, Bandyopadhyay R, Soni B (2022) Naturally occurring bentonite clay: structural augmentation, characterization and application as catalyst. Materials Today: Proceedings 57:194–201

Ghorbani M, Shams A, Seyedin O, AfsharLahoori N (2017) Magnetic ethylene diamine-functionalized graphene oxide as novel sorbent for removal of lead and cadmium ions from wastewater samples. Environ Sci Pollut Res 25:5655–5667

Ghorbani M, Seyedin O, Aghamohammadhassan M (2020) Adsorptive removal of lead (II) ion from water and wastewater media using carbon-based nanomaterials as unique sorbents: a review. J Environ Manage 254:109814

Ghorbani M, Ariavand S, Aghamohammadhasan M, Seyedin O (2021a) Synthesis and optimization of a green and efficient sorbent for removal of three heavy metal ions from wastewater samples: kinetic, thermodynamic, and isotherm studies. J Iran Chem Soc 18:1947–1963

Ghorbani M, Mohammadi P, Keshavarzi M, Saghi MH, Mohammadi M, Shams A, Aghamohammadhasan M (2021b) Simultaneous determination of organophosphorus pesticides residues in vegetable, fruit juice, and milk samples with magnetic dispersive micro solid-phase extraction and chromatographic method; recruitment of simplex lattice mixture design for optimization of novel sorbent composites. Analytica Chimica Acta 1178:338802

Gordi Z, Ghorbani M, AhmadianKhakhiyani M (2020) Adsorptive removal of enrofloxacin with magnetic functionalized graphene oxide@ metal-organic frameworks employing D-optimal mixture design. Water Environ Res 92:1935–1947

Guo Y, Zhao L, Ma Q, Ji C (2021) Novel strategies for degradation of aflatoxins in food and feed: a review. Food Res Int 140:109878

Ibrahim H, Sazali N, Ibrahim I, Sharip M (2019): Nano-structured cellulose as green adsorbents for water purification: a mini review. J Appl Membrane Sci Technol 23

Ismaeel SH, Mabrouk MS, Ali AA-A, Abn-Elwalead K (2017) Synthesis and characterization of bentonite nanocomposites from Egyptian bentonite clay. Nanotechnology 1:16–29

Ji J, Xie W (2021) Removal of aflatoxin B1 from contaminated peanut oils using magnetic attapulgite. Food Chem 339:128072

Li Y, Liu J, Yuan Q, Tang H, Yu F, Lv X (2016) A green adsorbent derived from banana peel for highly effective removal of heavy metal ions from water. RSC Adv 6:45041–45048

Li Y, Zhou Y, Wang R, Chen Z, Luo X, Wang L, Zhao X, Zhang C, Yu P (2022) Removal of aflatoxin B1 from aqueous solution using amino-grafted magnetic mesoporous silica prepared from rice husk. Food Chemistry 389:132987

Ma F, Cai X, Mao J, Yu L, Li P (2021) Adsorptive removal of aflatoxin B1 from vegetable oils via novel adsorbents derived from a metal-organic framework. J Hazard Mater 412:125170

Mahato DK, Lee KE, Kamle M, Devi S, Dewangan KN, Kumar P, Kang SG (2019) Aflatoxins in food and feed: an overview on prevalence, detection and control strategies. Front Microbiol 10:2266

Mohajeri P, Smith C, Selamat MR, Abdul Aziz H (2018) Enhancing the adsorption of lead (II) by bentonite enriched with pH-adjusted meranti sawdust. Water 10(12):1875

Negash D (2018) A review of aflatoxin: occurrence, prevention, and gaps in both food and feed safety. J Appl Microbiol Res 1:35–43

Pedram-Rad T, Es' haghi Z, Ahmadpour A (2019) Adsorptive desulfurization of model gasoline by using modified bentonite. J Sulfur Chem 40:149–165

Picardo M, Filatova D, Nunez O, Farré M (2019) Recent advances in the detection of natural toxins in freshwater environments. TrAC, Trends Anal Chem 112:75–86

Samuel MS, Kirankumar V, Selvarajan E (2021) Fabrication of a metal-organic framework composite for removal of Aflatoxin B1 from water. J Environ Chem Eng 9:104966

Shahmirzadi MAA, Hosseini SS, Luo J, Ortiz I (2018) Significance, evolution and recent advances in adsorption technology, materials and processes for desalination, water softening and salt removal. J Environ Manage 215:324–344

Vieira WT, de Farias MB, Spaolonzi MP, da Silva MGC, Vieira MGA (2020) Removal of endocrine disruptors in waters by adsorption, membrane filtration and biodegradation. A Review Environ Chem Lett 18:1113–1143

Wang S-Y, Herrera-Balandrano DD, Shi X-C, Chen X, Liu F-Q, Laborda P (2023): Occurrence of aflatoxins in water and decontamination strategies: a review. Water Res 119703

Wangia RN, Tang L, Wang J-S (2019) Occupational exposure to aflatoxins and health outcomes: a review. J Environ Sci Health C 37:215–234

Publisher's Note Springer Nature remains neutral with regard to jurisdictional claims in published maps and institutional affiliations.

Springer Nature or its licensor (e.g. a society or other partner) holds exclusive rights to this article under a publishing agreement with the author(s) or other rightsholder(s); author self-archiving of the accepted manuscript version of this article is solely governed by the terms of such publishing agreement and applicable law.